

Computational Investigation of the Interaction Between Hydrogen Atoms and an Intense Circularly Polarized Laser Field

Lifeng Yang^{1,2}, Wang Xu^{1,*}, Qiren Zhang³, Wen Luo^{1,2},
Qiangyan Pan¹, Xiaolu Cai^{1,2}, Gongtao Fan^{1,2}, Yongjiang Li^{1,2},
Benji Xu¹, Zhe Yan¹, Guangwei Fan^{1,2} and Zhendong An^{1,2}

¹ Shanghai Institute of Applied Physics, Chinese Academy of Sciences,
Shanghai 201800, China.

² Graduate School of the Chinese Academy of Sciences, Beijing 10039, China.

³ Departments of Technical Physics, Peking University, Beijing 100871, China.

Received 13 November 2010; Accepted (in revised version) 15 April 2011

Communicated by Zhengming Sheng

Available online 28 October 2011

Abstract. The study of interactions between a high-power laser and atoms has been one of the fundamental and interesting topics in strong field physics for decades. Based on a nonperturbative model, ten years ago, we developed a set of programs to facilitate the study of interactions between a circularly polarized laser and atomic hydrogen. These programs included only contribution from the bound states of the hydrogen atom. However, as the laser intensity increases, contribution from continuum states to the excitation and ionization processes becomes larger and can no longer be neglected. Furthermore, because the original code is not able to add this contribution directly due to its many disadvantages, a major upgrade of the code is required before including the contribution from continuum states in future. In this paper, first we deduce some important formulas for contribution of continuum states and present modifications and tests for the upgraded code in detail. Second we show some comparisons among new results, old results from the original codes and the available experimental data. Overall the new result agrees with experimental data well. Last we present our calculation of above-threshold ionization (ATI) rate and compare it with a perturbative calculation. The comparison shows that our nonperturbative calculation can also produce ATI peak suppression.

PACS: 32.80.Fb, 42.50.Hz, 32.80Rm

Key words: Hydrogen atoms, high-power laser, nonperturbative, photoionization.

*Corresponding author. *Email address:* xuwang@sinap.ac.cn (W. Xu)

1 Introduction

The study of interaction between a strong laser field and atoms originated from the perturbation theoretical study for two-photon transition by Göppert-Mayer [1] in 1931. However, the first experimental observation of atomic multiphoton ionization (MPI) [2,3] only took place in late 1960 after the laser was invented [4]. In early experiments, laser intensity ($I < 10^{12} \text{W/cm}^2$) was much lower than atomic coulomb field (10^{16}W/cm^2). Therefore, the MPI could be accurately described by Low Order Perturbation Theory (LOPT) [5–7]. However, LOPT has difficulties in explaining some nonperturbative phenomena such as near-resonant MPI [8], and AC Stark shift of atomic energy levels [9], which occurs when the laser intensity was sufficiently high. Although the perturbation theory included higher order perturbation extensions to explain these phenomena, it has already become necessary to study these phenomena under nonperturbative framework. In fact, the nonperturbative era for the study of interaction between a strong laser field and atoms did not truly begin until Above Threshold Ionization (ATI), a nonperturbative phenomenon, was discovered by P. Agostini from studying the interaction between a laser field and atomic silver [10] in 1979. Since then, many other new nonperturbative phenomena such as High Harmonic Generation (HHG) [11–14] and Stabilization [15–18] were discovered. In the past two years, due to the breakthrough of high-power and long-wave laser techniques [19], Low-Energy Structures (LES) [20,21], another novel nonperturbative phenomenon, was discovered. In addition, the study of atomic behavior in a field of the ultra-short super intense laser [22–24] recently became possible because of the development of ultra-short free electron lasers (FELs) in the extreme ultraviolet (XUV) to hard- x -ray wavelength regime [25,26]. More new nonperturbative phenomena are therefore expected to be observed in the near future. Because of all these, we foresee the study the interactions between high-power lasers and atoms to continue for decades.

Due to the simplicity of the hydrogen atom, there have been some experimental studies on the interaction of an intense laser with hydrogen atoms [27–31]. Although linearly polarized lasers, rather than circularly polarized lasers, are typically used in these experiments, the theoretical study of the interactions between circularly polarized lasers and hydrogen atoms is a basic topic and an important component in strong field physics. The earliest of such studies using nonperturbative theory is from the Keldysh-Faisal-Reiss (KFR) type theories based on strong field approximation in 1980s [32]. In the late 1980s, the Floquet theory was used in those studies [33–35]. In recent years, some theoretical physicists have directly solved two-dimension (2D) and three-dimension (3D) cases of the time-dependent Schrodinger equation (TDSE) of hydrogen atoms in an intense circularly polarized laser field [36–39]. We have focused on this study for more than a decade as well. Based on non-relativistic and dipole approximation, we built a nonperturbative model for solving the TDSE of hydrogen atom in a circularly polarized laser field [40,41]. Using this model and the Jacobi algorithm, we developed a FORTRAN program (Q1) with quadruple precision to facilitate this study. Later on, we upgraded Q1 to another FORTRAN program (Q2) by replacing the Jacobi algorithm with the Givens algorithm

to reduce calculation time. With code Q1 and code Q2, we performed many studies of interaction between a circularly polarized laser field and atomic hydrogen, which can be summarized as follows: with Q1, we studied atomic hydrogen behaviors in a circularly polarized laser field [42], the ionization process of hydrogen atoms in a circularly polarized standing wave [43], and made preliminary interpretations for the Kapitza-Dirac effect observed in experiment [44]; with Q2, we studied the behaviors of hydrogen atom, such as excitation and ionization, with respect to intensity of circularly polarized laser and predicted the nonperturbative phenomenon of non-integral quantum transition [45].

However, there are five main limitations in programs Q1 and Q2 [42–45]. Firstly, there is an overflow/underflow issue. When it occurs, eigenvalues will be calculated incorrectly. Secondly, some degenerate eigenvectors may appear under certain conditions. Due to these degenerate eigenvectors, if transitions between degenerate states occur, it is impossible to use Q1 and Q2 correctly study the interaction between a laser and atoms. Thirdly, both algorithms utilized to calculate eigenvalues and eigenvectors in Q1 and Q2 consume too much time. Both Q1 and Q2 are not able to calculate a matrix with an order of $n_b \times n_b$, where $n_b > 2109$ ($n_b = n_{\max}(n_{\max} + 1)(2n_{\max} + 1)/6$), where n_{\max} is the maximum principal quantum number of a set of basis vectors. Fourthly, as laser intensity increases, due to Tunneling Ionization (TI) or even Over Barrier Ionization (OBI) contributions of continuum states in the excitation and ionization processes can no longer be ignored [46, 47]. However, the effect of continuum states is not taken into account in Q1 and Q2, as only the bound states of hydrogen are considered in the theoretical models on which the two programs were build. Therefore, our original study for MPI (and ATI) based on Q1 and Q2 will not be conclusive if laser intensity is too high. Finally, although these two programs (Q1 and Q2) support high (quadruple) precision and can run on a supercomputer, they are difficult to troubleshoot and maintain. Also, the code is not portable because it was written for a supercomputer.

In order to resolve these disadvantages in the second program (Q2), we have tried a few solutions. First, in the new upgraded code (D), we incorporated an updated implementation of the Bisection algorithm [48]. The number of agreements in the signs of consecutive members of the leading principal minor Sturm sequence can be counted correctly in the new implementation of the Bisection algorithm. The overflow/underflow issue, therefore, disappears. Second, a small constant is employed in the Bisection algorithm of Q2 (see in subsection 3.2). From this perturbative Bisection algorithm, degenerate eigenvalues are split slightly among each other so that eigenvectors of these degenerate energies are different, perpendicular, and therefore eigenvectors are calculated correctly. Third, we modified the structure of code Q2 and optimized the implementation of the Bisection algorithm [48] (see subsection 3.1). Our tests show that the performance improved and eigenvalues are able to be calculated from a higher order matrix ($> 2109 \times 2109$, where $n_{\max} = 18$) of effective Hamilton H_e . Fourth, we have deduced some formulas for adding the contribution of hydrogen atomic continuum states in our model (see subsection 3.2). In the near future, we will incorporate these formulas into our code so that we can study the contributions from the continuum states. Lastly, we have mod-

ified Q2 to support double precision (D), which can run on a personal computer (PC) and possesses good compatibility and portability (see subsection 3.3). Our tests show that compared with Q2, the precision of results generated with D has not reduced, while execution speed improved significantly.

The remainder of this paper is organized as follows. Section II briefly introduces our theoretical model for both the bound states and continuum states of hydrogen atom. Section III discusses the upgrade and the improvements of the new program D and its advantages. Section IV reviews the results from this upgraded program and compares them with those from the original programs (Q1 and Q2) and the experimental result. Section V provides a summary and an outlook.

2 Theoretical model

Contributions from both bound and continuum states need to be considered for the wave function of a hydrogen atom in a very intense circularly polarized laser field. We leverage our past research to deduce the required formulas.

Firstly, let us briefly review the past work. In [41] and [42], we provided proof that in the Coulomb gauge and dipole approximation, the time dependent Schrödinger equation (TDSE) of a hydrogen atom under effects of both an intense circularly polarized laser field and Coulomb field can be transformed and written as:

$$H_e \psi_i(r) = E_i \psi_i(r), \quad (2.1)$$

where

$$H_e = \frac{p^2}{2m_e} + V(r) - \frac{k}{m_e} p_z l_z + \frac{k}{2m_e} l_z^2 + \frac{e^2 A^2}{2m_e} + \frac{eA}{m_e} p_x + kcl_z, \quad (2.2)$$

and $\psi_i(r)$ is the eigenfunction of H_e . $V(r) = -\alpha\hbar c/r$ is the Coulomb potential of hydrogen atom, α is the fine structure constant. $-e$ and m_e are electron charge and mass, k and A are wave number and the amplitude of vector potential for a circularly polarized laser. p is the momentum operator of electron, p_x and p_z are the momentum projection operator in x and z direction. l_z is the z component of the orbital angular momentum L for electron. The eigenfunction $\psi_i(r)$ can also be expanded in a complete set of basis vectors as:

$$\psi_i(r) \approx \sum_i C_{nlm}(i) \phi_{nlm}(r) \triangleq \psi_i^b(r), \quad (2.3)$$

where bound states $\phi_{nlm}(r)$ of hydrogen atom are only considered in our previous work and therefore these basis vectors are not complete. n , l and m are principal, angular, and magnetic quantum number respectively. In a weak laser field, this approximation is sufficient, but it is inadequate in an intense laser field. $C_{nlm}(i)$ is the coefficient of the expanded basis vectors $\phi_{nlm}(r)$ and can be obtained through a linear variation method.

\triangleq sign represents a definition operator. $\phi_{nlm}(r)$ is well known and can be written as: $\phi_{nlm}(r) = R_{nl}(r)Y_{lm}(\theta, \varphi)$. Here,

$$R_{nl}(r) = \frac{i^l}{(2l+1)!} \sqrt{\frac{(n+l)!}{2n(n-l-1)!}} \left(\frac{2}{n}\right)^{l+\frac{3}{2}} \times r^l e^{-\frac{r}{n}} {}_1F_1\left(l+1-n, 2l+2, \frac{2}{n}r\right), \quad (2.4)$$

where ${}_1F_1$ is confluent hypergeometric function. It is worth mentioning two special cases for Eq. (2.2):

Case 1) As the laser parameters $A = 0$ and $k = 0$, Eq. (2.2) can be simplified as: $H_e = p^2/2m_e + V(r)$. The eigenfunction $\psi_i(r)$ becomes one of the bound states $\phi_{nlm}(r)$.

Case 2) As the laser parameters $A=0$ and $k \neq 0$, Eq. (2.2) can be simplified as $H_e = p^2/2m_e + V(r) - kp_z l_z / m_e + kl_z^2 / 2m_e + kcl_z$. The eigenfunction $\psi_i(r)$ becomes one of the bound states $\phi_{n'l'}$.

These two cases have been utilized-in testing our new upgraded code. Because $\psi_i(r)$ is obtained from the wave function of hydrogen atom in an intense laser field by two unitary transformations ($\exp(i\omega l_z t / \hbar)$ and $\exp(-ikz l_z / \hbar)$), the hydrogen atomic wave function in a laser field can be expanded as:

$$\begin{aligned} \Psi(r, t) &= e^{\frac{i\omega l_z t}{\hbar}} e^{-\frac{ikz l_z t}{\hbar}} \sum_i C_{nlm}(i) \psi_i^b(r) e^{-\frac{iE_i t}{\hbar}} \\ &= \sum_{E'l'm'} \sum_i C_{nlm}(i) C_{E'l'm'}(i) \phi_{nlm}(r) e^{-\frac{i(E_i - m' \hbar \omega) t}{\hbar}} e^{-im'kz}. \end{aligned} \quad (2.5)$$

Therefore, the transition probability from the initial state $\phi_{n'l'm'}(r)$ to the final state $\phi_{nlm}(r)$ can be derived by:

$$W_{nlm, n'l'm'} = \sum_i C_{nlm}^2(i) C_{E'l'm'}^2(i). \quad (2.6)$$

In addition, under a certain laser intensity (where A and k are fixed), the photoionization rate per unit solid angle and unit time is (details see [42]).

$$\frac{dR_\mu}{d\Omega} = \frac{2\pi}{\hbar} \left| \left\langle f0\mu \left| \frac{eA}{m_e} [p_x \cos(kz) + p_y \sin(kz)] + \frac{e^2 A^2}{2m_e} |i \right\rangle \right| \rho. \quad (2.7)$$

Here, $|i\rangle$ represents the wave function of in-state

$$\Phi(r) = \sum_i \Phi_i^b(r) = \sum_i \exp\left(-\frac{ikz l_z}{\hbar}\right) \psi_i^b(r).$$

When the laser intensity is not sufficient high, the in-state $|i\rangle$ can be approximated to $\Phi(r) = \Phi_i^b(r) = \psi_i^b(r)$ under the long wavelength condition: $k \gg \alpha_0$, where α_0 is Bohr radius. The number N of absorbed photons is roughly equal to the change of magnetic

quantum number- μ between the initial ground state and final state of hydrogen atom. μ is the magnetic quantum number of the final state $|f0\mu\rangle$. However, the approximation of $N = -\mu$ is not true, when the laser intensity enough high. $\rho = k_e/8\pi^3\hbar^3$ is the density of final state at $E_f(E_f = E_i)$. Here $k_e = m_e\sqrt{2m_eE_{f0}}$ is the electron wave vector, where $E_{f0}(= E_i - \mu\hbar\omega)$ is the energy of $|f0\mu\rangle$. According to the photoionization rate $dR_\mu/d\Omega$, the differential cross section $d\sigma_\mu/d\Omega$ can be formulized as:

$$\frac{d\sigma_\mu}{d\Omega} = \frac{1}{J} \frac{dR_\mu}{d\Omega} = \frac{A^2k}{\hbar\mu_0} \frac{dR_\mu}{d\Omega}. \quad (2.8)$$

Here, J is the incident photon number per unit time (laser intensity $I = \varepsilon_0 A^2 k^2 c^3 / 2$). ε_0 and μ_0 are vacuum conductivity and permeability. The photoionization differential cross section $d\sigma_\mu(\Theta)/d\Theta$ derived from Eqs. (2.7) and (2.8) can be given as:

$$\frac{d\sigma_\mu(\Theta)}{d\Theta} = \frac{16\pi\alpha v_e}{\hbar^2\omega} \int_0^{2\pi} \left| \sum_i \alpha_{i'} Y_{i'\mu}(\Theta, \Phi) \right|^2 \times \sin\Theta d\Phi. \quad (2.9)$$

Here, $v_e = \sqrt{E_{f0}}/\hbar$ is the velocity of the photoelectron, both (k_e, Θ, Φ) and (r, θ, φ) are the spherical coordinates of momentum space and position space, α is the fine structure constant, and

$$\alpha_{i'} = (-i)^{i'} \int j_{i'}(k_e r) Y_{i'\mu}(\theta, \varphi) \times \left[p_x \cos(kz) + p_y \sin(kz) + \frac{1}{2} eA \right] \Phi_i^b(r) d\vec{r}. \quad (2.10)$$

The total photoionization cross section σ_μ (the unit is $\pi\alpha_0^2$) for photoelectron with magnetic quantum number μ can be obtained from Eq. (2.9) as:

$$\sigma_\mu = \frac{16\alpha^2 k_e}{k} \sum_{i'=|\mu|} |\beta_{i'}(i)|^2, \quad (2.11)$$

where $\beta_{i'} = \alpha_{i'}/(\hbar\sqrt{\alpha_0})$. Moreover, according to integral of Eqs. (2.8) and (2.11), the total photoionization rate R_μ can be derived by:

$$R_\mu = \frac{8\alpha\varepsilon_0^2 A^2 k_e c}{\pi\hbar^2 \alpha_0^2} \sum_{i'=|\mu|} |\beta_{i'}(i)|^2. \quad (2.12)$$

The corresponding photoelectron ionization yield for a time period t is

$$N_e = R_\mu \times t \times N_H = \frac{8\alpha\varepsilon_0^2 A^2 k_e c t N_H}{\pi\hbar^2 \alpha_0^2} \sum_{i'=|\mu|} |\beta_{i'}(i)|^2. \quad (2.13)$$

Here, $N_H = \pi \times W^2 \times T_p \times c \times \rho_H$ is the total number of interacting hydrogen atoms, where T_p is the laser pulse length if a pulsed laser is used, W is the laser beam waist, and ρ_H is the effective density of atomic hydrogen.

Secondly, the above formulas are however not fully valid in a very intense laser field. In order to obtain the correct the wave function of hydrogen atom in a very intense circularly polarized laser field, we can simply add the continuum states into a set of the basis vectors $\{\phi_{nl\mu}(i)\}$ from Eq. (2.3). Thus, we can rewrite the Eq. (2.3) as:

$$\psi_i(r) = \sum_{nlm} C_{nlm}(i) \phi_{nlm}(r) + \int \sum_{E'l'm'} C_{E'l'm'}(i) \varphi_{E'l'm'}(r) dE \triangleq \psi_i^b(r) + \psi_i^c(r). \quad (2.14)$$

Here $\varphi_{E'l'm'}$ is the continuum state of hydrogen atom. If energy E is discrete, $\psi_i^c(r) = \sum_{Elm} \Delta E \cdot C_{Elm}(i) \varphi_{Elm}(r)$. $C_{E'l'm'}(i)$ and $C_{nlm}(i)$ are the coefficient of the basis vectors, $\varphi_{E'l'm'}(r)$ and $\varphi_{n(E)lm}(r)$, respectively. $\varphi_{Elm}(r) = R_{El}(r) Y_{lm}(\theta, \varphi)$, where

$$R_{El}(r) = \frac{1}{(2l+1)!} \prod_{q=1}^l (q^2 + w^2)^{\frac{1}{2}} \left[\frac{1}{1 - e^{2\pi w}} \frac{w}{k} \right]^{\frac{1}{2}} \times (2kr)^{l+1} e^{ikr} F(l+1 - iw, 2l+2, -2ikr). \quad (2.15)$$

Here, $k = \sqrt{2mE}$ and $w = 1/(\alpha_0 \sqrt{2mE})$. Similar to Eq. (2.5) which is based on bound states, we can derive the wave function of hydrogen atom as:

$$\Psi(r, t) = \sum_i C_{nlm}(i) \psi_i(r) e^{-\frac{iE_i t}{\hbar}} e^{im_l \omega t} e^{-\frac{im_k z}{\hbar}} + \int_0^\infty \sum_{Elm} C_{Elm}(i) \psi_i(r) e^{-\frac{iE t}{\hbar}} e^{im \omega t} e^{-\frac{im_k z}{\hbar}} dE. \quad (2.16)$$

The transition rate from the initial state $\varphi_{n'(E')l'm'}(r)$ to the final state $\phi_{nlm}(r)$ can therefore be written as (if energy E is discrete):

$$W_{nlm, n'(E')l'm'} = \sum_i C_{nl\mu}^2(i) C_{n'(E')l'm'}^2(i) (\Delta E)^2. \quad (2.17)$$

Accordingly, the other photoionization formulas can retain the same format if we simply replace $\Phi_i^b(r)$ with $\Phi_i^b(r) + \Phi_i^c(r)$, where $\Phi_i^c(r) = \exp(-ik_z l_z / \hbar) \psi_i^c(r)$.

Finally, we should also consider the energy cut off and the energy gap (i.e., how to choose ΔE) to write a computational program practically. In order to correctly incorporate the contribution of continuum states into Q2 in future, additional formulas need to be deduced.

The next three sub-sections (subsections 3.1, 3.2 and 3.3) will describe how we improved the calculation for eigenvalues, eigenvectors and the calculation time, respectively. The detailed verifications and advantages of the new program D will be introduced in the following subsections. In the next section, we will discuss the implementation and testing of the upgrades.

3 The upgrade program and its advantages

Before going into the detailed works for the upgraded program D, we will first briefly introduce the structure of the original code Q2 and the upgraded code D. The left panel of Fig. 1 shows the flow chart of the code Q2. Its overall process can be described as follows:

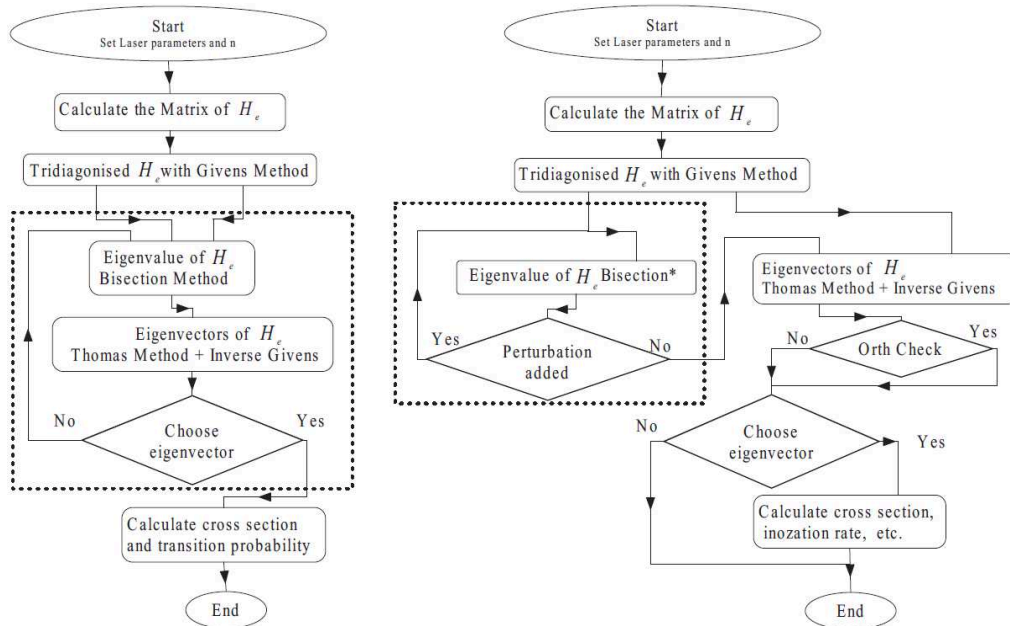


Figure 1: Flowcharts of the codes: Q2 (left) and D (right).

1) calculating the effective Hamiltonian matrix H_e of the hydrogen atom in a circularly polarized laser field, 2) tridiagonalizing the H_e with the Givens method, 3) calculating an eigenvalue of the tridiagonal matrix using the Bisection algorithm [49,50], 4) calculating the corresponding eigenvector using the Thomas algorithm [51] and Givens inverse transformation, 5) checking whether this eigenvector is needed, and if not going back to 3), otherwise advance to 6), and 6) calculating and outputting some physical results, such as the photoionization cross section and transition probability. The right panel of Fig. 1 shows the flow chart of the upgraded code D. In Q2, once an eigenvalue is obtained, the corresponding eigenvector will be calculated immediately. In D, we modified the procedure to first calculate all eigenvalues at once, then all the eigenvectors in order to help us examine both eigenvalues and eigenvectors. The adjusted flow chart is shown in the dotted frame of the right panel of Fig. 1.

3.1 Improvements to eigenvalue calculation

The accuracies of eigenvalues directly affect the accuracies of eigenvectors. However, sometimes eigenvalues cannot be correctly calculated by Q2, leading to inaccurate eigenvectors. After we modified code Q2 to use double precision and verified the calculation of eigenvalues. We performed three validations.

First, we consider the case where both parameters of A and k are 0. In this case, the effective Hamiltonian H_e becomes just the standard Hamiltonian of the hydrogen atom.

Thus, the corresponding eigenvalue is expected as $E = \alpha^2 m_e c^2 / 2n^2$, where n is the principal quantum number. However, the value of the quadratic polynomial is sometimes over the limit of the precision of the parameter in a certain calculation cycle. Therefore, the number of agreements in sign of consecutive members of polynomial Sturm sequence cannot be counted correctly in the procedure of the Bisection algorithm [49, 50]. The issue of overflow or underflow will occur and the eigenvalues will be calculated incorrectly. The relative difference between calculated eigenvalue from Q2 and the expected value can be in the hundreds. In order to resolve this issue, in the new code D, we replace the implementation of the Bisection algorithm with an updated one [48]. The calculated eigenvalues from program D are very close to the expected values. Their relative differences are as small as 0.04%. We conclude that D behaves properly when parameters A and k are 0 due to the new implementation of the Bisection algorithm.

Second, we consider the case where the laser parameters are $A = 0$ and $k > 0$. For example, the eigenvalues of H_e listed in Table 1 are calculated from the code D for $k = 1.0 \times 10^7 \text{m}^{-1}$. The calculated eigenvalues are consistent with our expectations. When the magnetic quantum number m is 0 and the principal quantum number n is fixed, the degeneracies of eigenvalues occur for different angular quantum number l . The corresponding eigenvalue is very close to $E = \alpha^2 m_e c^2 / 2n^2$. We conclude that program D can work well with parameters $A = 0$ and $k > 0$. Last, we consider the case where the laser parameters $A > 0$ and $k > 0$. As an example, we computed the eigenvalues of H_e listed in Table 2 from programs D and Q2 for the laser wavelength of $10.64 \mu\text{m}$ and $n_{\text{max}} = 12$. Table 2 shows that the eigenvalues of H_e from D and from Q2 are same. We conclude that program D can also work as expected with parameters $A > 0$ and $k > 0$.

Table 1: The calculated eigenvalues with $n_{\text{max}} = 5$ and nlm are principal, orbital angular momentum, and magnetic quantum numbers, respectively.

$A=0$	$A=0, k=0$			$A=0$	$A=0, k=0$				
$k=1.0 \times 10^7 \text{m}^{-1}$	$\alpha^2 m_e c^2 / 2n^2$	n	l	m	$k=1.0 \times 10^7 \text{m}^{-1}$	$\alpha^2 m_e c^2 / 2n^2$	n	l	m
-13.61eV	-13.60eV	1	0	0	-0.8504eV	-0.8500eV	4	2	0
-3.401eV	-3.400eV	2	0	0	-0.8504eV	-0.8500eV	4	3	0
-3.401eV	-3.400eV	2	1	0	-0.5442eV	-0.5440eV	5	0	0
-1.512eV	-1.511eV	3	0	0	-0.5442eV	-0.5440eV	5	1	0
-1.512eV	-1.511eV	3	1	0	-0.5442eV	-0.5440eV	5	2	0
-1.512eV	-1.511eV	3	2	0	-0.5442eV	-0.5440eV	5	3	0
-0.8504eV	-0.8500eV	4	0	0	-0.5442eV	-0.5440eV	5	4	0
-0.8504eV	-0.8500eV	4	1	0					

Table 2: The calculated eigenvalues of H_e from the code D and code Q2.

$I(10^{12} \text{W} \cdot \text{cm}^{-2})$	D	Q2	$I(10^{12} \text{W} \cdot \text{cm}^{-2})$	D	Q2
1.0	0.3618eV	0.3618eV	3.5	40.75eV	40.75eV
2.3	21.79eV	21.79eV	4.2	54.18eV	54.18eV

In conclusion, the overflow/underflow issue is successfully resolved in the upgraded program D. The eigenvalues calculated from D are demonstrated to be correct in three different cases of laser parameters.

3.2 Improvements to eigenvector calculation

The accuracy of eigenvectors is a key verification because it directly affects physical outputs such as photoionization cross section and transition probability. Eigenvector calculation in Q2 is performed with the Thomas algorithm [51]. As the eigenvalues are well-separated, the corresponding eigenvectors can be calculated correctly with the Thomas algorithm. All eigenvectors are should be perpendicular with each other. However, as some eigenvalues are identical, their corresponding degenerate eigenvectors are almost the same or parallel. These eigenvectors are therefore incorrect. In order to avoid the above issue, a small arbitrary constant, ε is employed in the Bisection algorithm of D. After this perturbative Bisection algorithm is used, the degenerate eigenvalues are slightly spread out. If becomes large, the splits among degenerate eigenvalues become large. As the splits become sufficiently large, degenerate eigenvectors begin to become perpendicular to each other while the eigenvalues become worse. In order to balance this, we study the relationship between and orthogonality of all eigenvectors O_{\max} . Here, $O_{\max} = \max\{\langle p|q\rangle\}$ represents the maximum value of inner product of any two different eigenvectors p , and q among all possible eigenvectors. From the left panel of Fig. 2, one can see that the optimized value of ε is around 10^{-6} , which can only affects the accuracies of eigenvalues in the order of 10^{-6} , the orthogonality of all eigenvectors O_{\max} will be better than 10^{-6} . In order to finalize this conclusion, having chosen ε of 10^{-6} , we have carefully checked orthogonality of all eigenvectors O_{\max} under different situations. In Fig. 3, a wide range of n_{\max} is employed, and different laser parameters (A and k) are used. This figure shows that over all the orthogonalities of all the eigenvectors O_{\max} are better than 10^{-6} . As a result, we conclude that if ε is set as 10^{-6} , both eigenvalues and

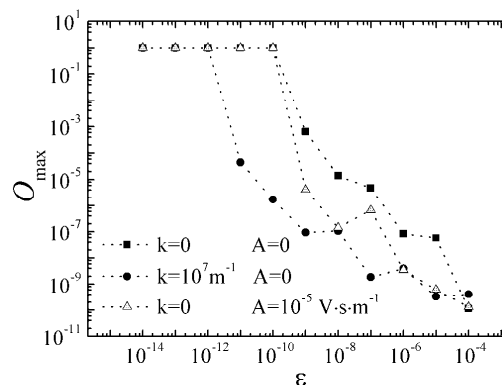


Figure 2: The orthogonality of all eigenvectors (O_{\max}) in terms of a small arbitrary constant ε for $n_{\max} = 18$.

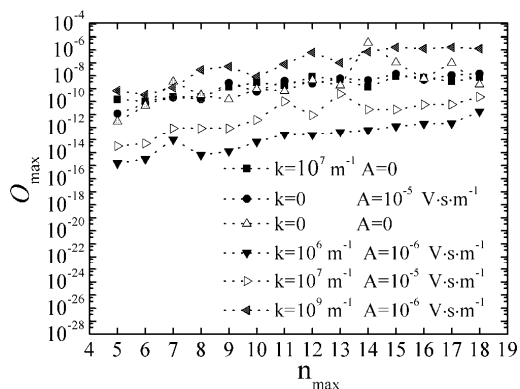


Figure 3: The orthogonality of all eigenvectors (O_{\max}) as a function of with different laser parameters n_{\max} (A and k).

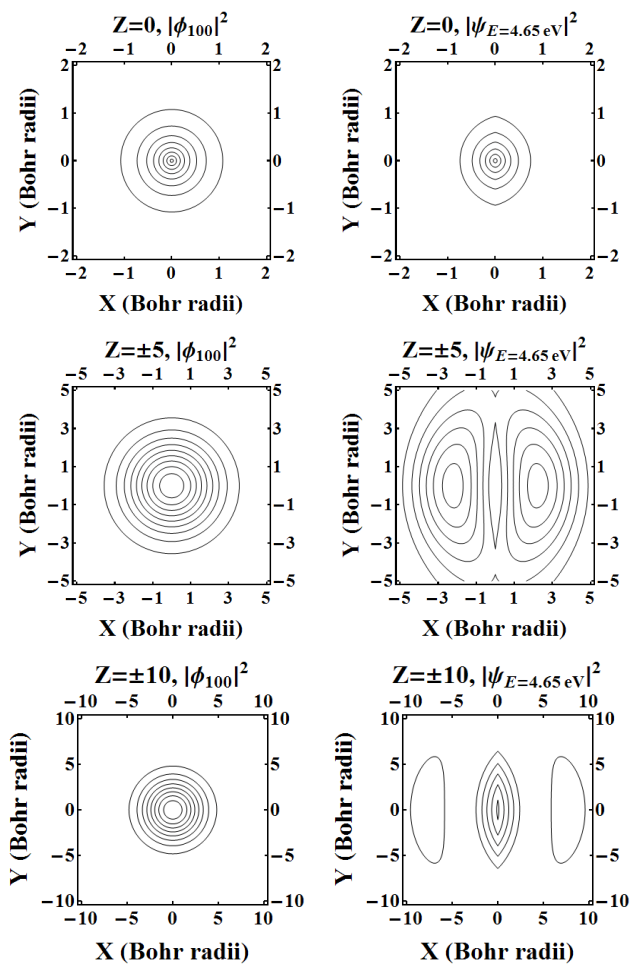


Figure 4: The contour plots of $|\phi_{100}|^2$ (left) and $|\psi_{E=4.65\text{eV}}|^2$ (right) with different z .

eigenvectors can be obtained with a precision of about 10^{-6} by employing the perturbative Bisection algorithm when the eigenvectors are degenerate.

After eigenvectors are calculated correctly by D, the eigenfunction $\psi_i(r)$ of H_e (see Eq. (2.3)) is calculated. As the laser parameters $A = 1.8 \times 10^{-5} \text{V} \cdot \text{s} \cdot \text{m}^{-1}$ and $\lambda = 1.64 \mu\text{m}$ and $n_{\text{max}} = 15$, the eigenfunction $\psi_{E=4.65\text{eV}}$, which has a largest component of ground state of hydrogen atom, is calculated with corresponding eigenenergy $E = 4.65\text{eV}$. In the presence of a circularly polarized laser field along Z direction, the ground state (ϕ_{100}) of a hydrogen atom will most likely evolve into $\psi_{E=4.65\text{eV}}$. From Fig. 4 we can see that the ground state of hydrogen atom ϕ_{11} has a spherical symmetry, but not the eigenfunction $\psi_{E=4.65\text{eV}}$. This means that in the presence of a circularly polarized a field along Z direction, a hydrogen atom at the ground state will lose its spherical symmetry. The higher the laser intensity, the more $\psi_{E=4.65\text{eV}}$ deforms. From this, we conclude that the eigenvectors calculated by program D are not only correct, but also reasonable in the physical context.

3.3 Improvements to calculation time

The calculation time is another key issue for the upgraded program, and is crucial for us as we consider adding the contribution from continuum states directly into D. Up to now; we have presented our work in modifying the original program Q2. The calculation time has been improved because we have adjusted the structure, algorithms and precision of the code. For example, using Q2, the calculation for 20 data points with $n_{\text{max}} = 18$ consumes about one week if without the overflow (or underflow) issue. On the contrary, using program D, the total run time for 20 data points is only about ten hours, taking about half an hour per data point $n_{\text{max}} = 18$ (see Fig. 5). Because the calculation speed is improved more than one order of magnitude and the overflow/underflow issue is resolved (the detailed is shown in subsection 3.1), the eigenvalues for the code D can be calculated from a higher order matrix ($> 2109 \times 2109$) of effective Hamiltonian H_e .

As an example, using the code D, we calculate photoionization cross section in terms

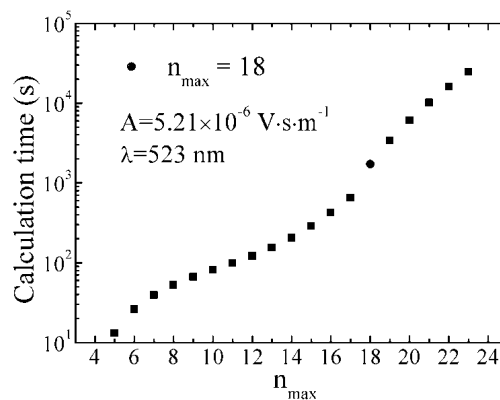


Figure 5: Calculation time of code D Vs. n_{max} .

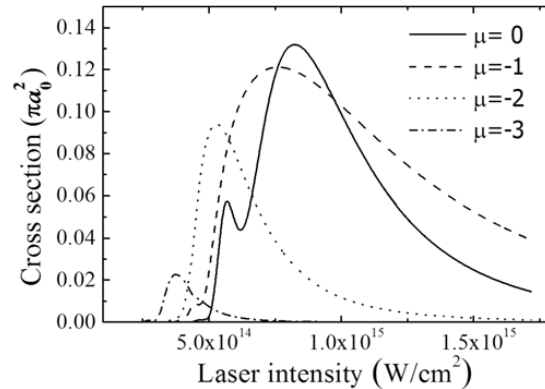


Figure 6: The photoionization cross section vs. laser intensity with wavelength of 523nm.

of laser intensity based on Eq. (2.11) (see Fig. 6). Here n_{\max} is set as 20 and is larger than 18 [45]. In Fig. 6, one can see that under high laser intensity the ground state of hydrogen atom can be ionized and the generated photoelectron is possibly with different magnetic quantum number μ . There are three ionization mechanisms: Multiphoton ionization (MPI), tunneling ionization (TI) and over the barrier ionization (OTBI) [52]. The laser intensity shown in Fig. 6 is ranges from 0.25 to 1.5PW/cm² ($I_{OTBI}=0.14PW/cm^2$). So the over-barrier ionization (OTBI) dominated this photoionization process.

Now program D is ready to provide some outputs. In the next section, we will generate more results from D and analyze them in a physical context.

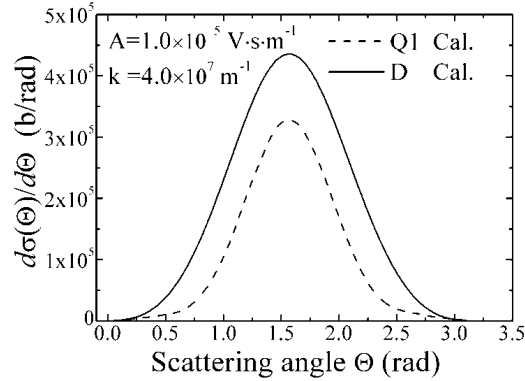
4 Result and discussion

From the above section, one can see that the upgraded code D not only has higher precision and reliability for eigenvalues and eigenvectors, but also largely reduces calculation time. In this section, we will give some physical calculations and compare the calculations with those from the original codes (Q1 and Q2) and available experimental results.

Firstly, with D, we calculate the differential photoionization cross sections and photoionization rates with different emission angles of photoelectron. If laser intensity is low enough and the perturbative approximation is valid, the change of magnetic quantum number $-\mu$ between initial and final states is approximated to the number N of absorbed photons. When a hydrogen atom absorbs one photon on average, the total one photon photoionization differential cross section from Eq. (2.9) can be obtained as:

$$\frac{d\sigma(\Theta)}{d\Theta} = \sum_N \frac{1}{N} \frac{d\sigma_{\mu=-N}(\Theta)}{d\Theta}. \quad (4.1)$$

Since the corresponding results from Q1 [42] are available but not Q2, using the same parameters in [42] we calculate $d\sigma(\Theta)/d\Theta$ (see Fig. 7) and photoionization rate (see Table

Figure 7: $d\sigma(\Theta)/d\Theta$ as a function of scattering angle Θ for $n_{\max}=5$.

3) with D, and compare them with those in [42]. From Fig. 7 and Table 3, we can see that there is same trend for the results from both code D and code Q1. On the other hand, there are some discrepancies between them. We cannot find good explanations for this. Possible explanations might be: 1) the code Q1 is our early developed code and its reliability might not be good; 2) the formulas for the average one photon photoionization differential cross section are not same in these two codes (we cannot find the formula in [42]).

Table 3: Photoionization rates ($R_{45^\circ}, R_{90^\circ}, R_{135^\circ}$) calculated with code D and code Q1 for the ground state of H_e at emission angles of 45, 90 and 135 degree, E_{f0} is the kinetic energy of photoelectron with magnetic quantum number μ . Parameters $k=3.32 \times 10^7 \text{ m}^{-1}$, $A=8.89 \times 10^{-6} \text{ V} \cdot \text{s} \cdot \text{m}^{-1}$ and $n_{\max}=5$ are used for the calculation.

μ	$E_{f0}(\text{eV})$		$R_{45^\circ}(\text{s}^{-1})$		$R_{90^\circ}(\text{s}^{-1})$		$R_{135^\circ}(\text{s}^{-1})$	
	D	Q1	D	Q1	D	Q1	D	Q1
-2	2.19	2.06	6.9×10^{13}	2.0×10^{14}	4.8×10^{14}	1.0×10^{15}	6.9×10^{13}	1.6×10^{14}
-3	8.75	8.48	2.5×10^{13}	5.7×10^{12}	2.8×10^{14}	4.2×10^{13}	2.5×10^{13}	4.9×10^{12}
-4	15.3	14.9	3.5×10^{10}	7.6×10^9	8.0×10^{11}	1.1×10^{11}	3.5×10^{10}	6.3×10^9
-5	21.8	21.3	2.8×10^5	8.3×10^4	1.3×10^7	2.6×10^6	2.8×10^5	8.3×10^4

Secondly, we calculate photoionization cross section from Eq. (2.11) and transition probability from Eq. (2.6), and compare them with those from length of $\lambda=10.64\mu\text{m}$ and $n_{\max}=12$ are employed in calculating the photoionization cross section with respect to laser intensity in both code D and code Q2 (see in Fig. 8). Also, the same laser wavelength of $\lambda=10.64\mu\text{m}$ and $n_{\max}=18$ are employed in calculating the transition probability from the ground state (100) of hydrogen atom to state (200) and state (21-1) with both D and Q2 [45] (see in Fig. 9). From the results shown in both Fig. 8 and Fig. 9, one can see that the calculated results from the two programs agree, differing only by less than 1% code Q2 in [45]. The comparisons show the good reliability of new code D.

Lastly, we try to compare the calculated photoelectron ionization yields of atomic

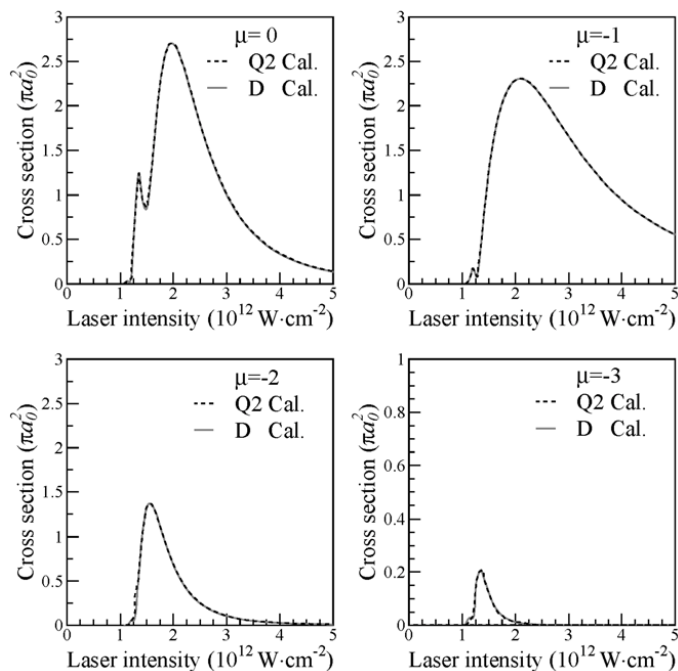


Figure 8: Ionization cross sections of $\mu=0, -1, -2$ and -3 as a function of laser intensity calculated by code Q2 and code D. The laser wavelength of $\lambda=10.64\mu\text{m}$ and $n_{\text{max}}=12$ are used for the calculation.

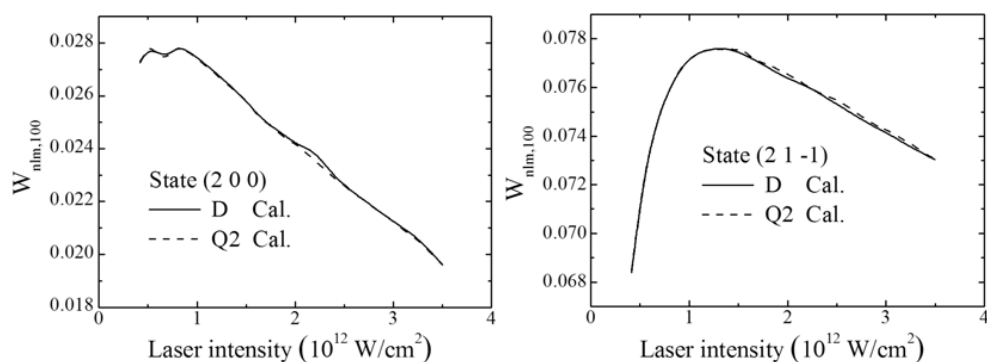


Figure 9: The transition probability $W_{nlm,100}$ from the ground state (100) of hydrogen atom to state (200) and state (21-1) as a function of the laser intensity. The laser wavelength of $10.64\mu\text{m}$ and $n_{\text{max}}=18$ is used for the calculation.

hydrogen from code D with the most recent experimental data. Existing theories show that there are some little difference ionization rate difference of hydrogen atom in an intense linear polarization laser and circular polarization laser [53]. Especially due to the lack of circular polarization data, we use the available experimental data of linear polarization [30] to compare with our model and other theories. Using the same parameters as those in [30] and setting $t = T_p$ and taking the waist radius of the laser beam to be

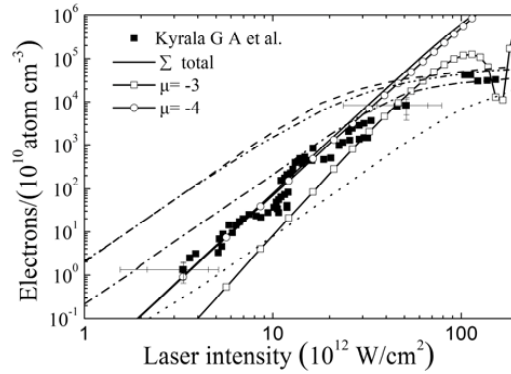


Figure 10: Comparison of electron production rates among theoretical and experimental results: solid square for experimental results (see [30]), dashed curve for the perturbative calculation (see [54]), dash-dot-dotted curve for the Floquet calculation (see [55]), dash-dotted curve for the Coulomb-corrected Keldysh calculation (see [56]) and dotted curve for the Keldysh calculation (see [56]) and Reiss (see [32]). Solid curve is for our work: solid curve for total ionization, solid curve with open circles for the $\mu = -4$ ionization and black solid curve with open squares for the $\mu = -3$ ionization. In our calculation the laser wavelength 248nm and $n_{\max} = 20$ are used.

$W = 45\mu\text{m}$, we calculate the yield of the photoelectron ionization (see Fig. 10) caused by the interaction of a circularly polarized laser with hydrogen atoms based on Eq. (2.13) with the upgraded code. The yield of the photoelectron ionization for all theoretical calculations and experimental data increases exponentially with the laser intensity in Fig. 10. The growth of experiment data slows down when the laser intensity is higher than $30\text{TW}/\text{cm}^2$. Overall, our nonperturbative calculation agrees with the experiment results best. As the laser intensity is greater than $30\text{TW}/\text{cm}^2$ and become larger, the agreement becomes worse due to the overestimation of our calculation. There may be two reasons. One is the contribution from continuum states for in-state and it cannot be neglected any more as laser intensity is high enough. The other is the contributions of laser field effect and coulomb effect for photoelectron [52] and they are also not negligible with high laser intensity. When the laser intensity is higher than $30\text{TW}/\text{cm}^2$, it is necessary to take into account the contributions mentioned above.

In addition, photoionization peak suppression is one of the interesting features of the Above-threshold ionization (ATI) in the domain of multiphoton ionization of atoms. The perturbative calculation for atomic hydrogen [58,59] is used as an analogy to explain the ATI peak suppression effect of Xenon in circularly polarized laser field [57,59].

Table 4 shows relative ATI rate of atomic hydrogen in an intense circularly polarized laser field with a wavelength of 532nm from the calculation by perturbation theory model and our nonperturbative theory model. $6+S$ means the atomic hydrogen absorbs $6+S$ photons in the multiphoton ionization process (MPI). Here, 6 represents the minimal number of photons for hydrogen atom ionization. In the perturbative calculation [59] (see column two and three in Table 4), the rate of $(6+0)$ ATI-0 becomes smaller than that of $(6+1)$ ATI-1 when the laser intensity is around $15\text{TW}/\text{cm}^2$. This means the ATI peak

Table 4: $(6+S)$ -photon ionization of hydrogen atom in a circularly polarized laser field with a wavelength of 532nm, normalized to that of the $S=0$ peak.

$6+S$	In [59] R_{6+S}/R_6		Our model R_{6+S}/R_6	
	10TW/cm ²	15TW/cm ²	5TW/cm ²	9TW/cm ²
$6+0$	1	1	1	1
$6+1$	0.892	1.31	0.1234	1.68
$6+2$	0.113	0.254	2.7E-7	7.0E-6
$6+3$	0.00723	0.0243	1.4E-13	6.58E-11
$6+4$	0.000319	0.00161	2.5E-20	2.02E-18

suppression effect occurs at the laser intensity of around 15TW/cm². According to our calculation for hydrogen atom (see column four and five in Table 4), the ATI peak suppression effect in domain of multiphoton ionization can also be explained. However the peak suppression effect occurs at the laser intensity of around 9TW/cm² other than 15TW/cm².

5 Conclusions and outlook

During the last decade, we developed a nonperturbative theoretical model and a set of FORTRAN programs to solve the TDSE of hydrogen atom in a circularly polarized laser field. We have carried out some calculations with these programs, such as atomic hydrogen photoionization in a circularly polarized laser field.

However, these programs have some limitations and therefore need to be upgraded. In this paper, we present the upgrade process in detail and test for its precision and reliability. These tests show that the upgraded code not only has high reliability and precision, but also largely reduces the calculation time. Using this code, we have also done some comparisons with the original codes and experimental data. All these comparisons show that the upgraded code is reasonable and our nonperturbative calculation can also produce the ATI peak suppression effect in domain of multiphoton ionization.

We have been stimulated by many new phenomena in strong field physics for decades. In the near future, we plan on incorporating contribution of continuum states into the updated code and extending our study more carefully to some physical processes in a high-power laser field, such as MPI and ATI. If possible, we would like to explore some new phenomena such as Stabilization and LES.

Acknowledgments

This work is supported by One Hundred Talents Project of Chinese Academy of Sciences (2006) (26010701), by Knowledge Innovation Project of Chinese Academy of Sciences (KJCX2-SW-N13) and by the National Natural Science Foundation of China (10675156).

References

- [1] M. Göppert-Mayer, *Ann. Phys.*, 9 (1931), 273–295.
- [2] G. S. Voronov and N. B. Delone, *Sov. Phys. JETP Lett.*, 1 (1965), 66.
- [3] P. Agostini et al., *IEEE J. Quantum Elect.*, 4 (1968), 667–669.
- [4] T. H. Maiman, *Nature*, 187 (1960), 493–494.
- [5] M. LuVan, G. Mainfray, C. Manus and I. Tugov, *Phys. Rev. A*, 7 (1973), 91–98.
- [6] F. Fabre, G. Petite, P. Agostini and M. Clement, *J. Phys. B*, 15 (1982), 1353.
- [7] G. Petite et al., *Phys. Rev. A*, 29 (1984), 2677–2689.
- [8] P. Lambropoulos, *Adv. At. Mol. Phys.*, 12 (1976), 87–164.
- [9] R. R. Freeman et al., *Phys. Rev. Lett.*, 59 (1987), 1092–1095.
- [10] P. Agostini et al., *Phys. Rev. Lett.*, 42 (1979), 1127–1130.
- [11] A. McPherson et al., *J. Opt. Soc. Am. B*, 4 (1987), 595–601.
- [12] M. Ferray et al., *J. Phys. B*, 21 (1988), L31–L35.
- [13] A. L’Huillier et al., in: *Multiphoton Processes*, ed. G. Mainfray, P. Agostini, Saclay, CEA, 1991, pp. 45.
- [14] P. B. Corkum, *Phys. Rev. Lett.*, 71 (1993), 1994–1997.
- [15] Q. Su, J. H. Eberly and J. Javanainen, *Phys. Rev. Lett.*, 64 (1990), 862–865.
- [16] J. H. Eberly and K. C. Kulander, *Science*, 262 (1993), 1229–1233.
- [17] N. J. van Druten et al., *Phys. Rev. A*, 55 (1997), 622–629.
- [18] B. Piraux and R. M. Potvliege, *Phys. Rev. A*, 57 (1998), 5009–5012.
- [19] P. Colosimo et al., *Nature Phys.*, 4 (2008), 386–389.
- [20] C. I. Bлага et al., *Nature Phys.*, 5 (2009), 335–338.
- [21] W. Quan et al., *Phys. Rev. Lett.*, 103 (2010), 093001.
- [22] J. Wark, *Nature*, 466 (2010), 35.
- [23] L. Young et al., *Nature*, 466 (2010), 56.
- [24] M. Meyer et al., *Phys. Rev. Lett.*, 104 (2010), 213001.
- [25] W. Ackermann et al., *Nature Photonics*, 1 (2007), 336–342.
- [26] P. Emma, in: *Proceedings of the 23rd Particle Accelerator Conference, Piscataway, Vancouver, Canada, 2009, TH3PBI01*.
- [27] D. E. Kelleher, M. Ligare and L. R. Brewer, *Phys. Rev. A*, 31 (1985), 2747–2749.
- [28] H. G. Muller et al., *Phys. Rev. A*, 34 (1986), 236–243.
- [29] H. Rottke, B. Wolff, M. Brickwedde, D. Feldmann and K. H. Welge, *Phys. Rev. Lett.*, 64 (1990), 404–407.
- [30] G. A. Kyrala and T. D. Nichols, *Phys. Rev. A*, 44 (1991), R1450–R1453.
- [31] H. Rottke et al., *Phys. Rev. A*, 49 (1994), 4837–4851.
- [32] H. R. Reiss, *Phys. Rev. A*, 22 (1980), 1786–1813.
- [33] R. Shakeshaft, R. M. Potvliege, M. Dörr and W. E. Cooke, *Phys. Rev. A*, 42 (1990), 1656–1668.
- [34] M. Dörr, R. M. Potvliege, D. Proulx and R. Shakeshaft, *Phys. Rev. A*, 43 (1991), 3729–3740.
- [35] R. M. Potvliege, in: *Atoms in Intense Laser Fields*, ed. M. Gavrilu, Academic, New York, 1992, pp. 373.
- [36] M. Pont and M. Gavrilu, *Phys. Rev. Lett.*, 65 (1990), 2362–2365.
- [37] W. Chism, D. I. Choi and L. E. Reich, *Phys. Rev. A*, 61 (2000), 054702.
- [38] D. I. Choi and W. Chism, *Phys. Rev. A*, 66 (2002), 025401.
- [39] M. Boca, H. G. Muller and M. Gavrilu, *J. Phys. B*, 37 (2004), 147.
- [40] Q. R. Zhang, *Commun. Theor. Phys.*, 28 (1997), 335.
- [41] Q. R. Zhang, *Phys. Lett. A*, 216 (1996), 125–128.

- [42] D. Zhang and Q. R. Zhang, *Commun. Theor. Phys.*, 36 (2001), 685.
- [43] X. T. Liu and Q. R. Zhang, *Commun. Theor. Phys.*, 41 (2004), 461–464.
- [44] C. L. Xiong and Q. R. Zhang, *Commun. Theor. Phys.*, 42 (2004), 891–894.
- [45] Q. R. Zhang, *Commun. Theor. Phys.*, 47 (2007), 1017–1023.
- [46] J. Grochmalicki, J. R. Kuklinski and M. Lewenstein, *J. Phys. B*, 19 (1986), 3649–3668.
- [47] N. B. Delone, S. P. Goreslavsky and V. P. Krainov, *J. Phys. B*, 22 (1989), 2941–2945.
- [48] W. Barth, R. S. Martin and H. J. Wilkinson, *Numer. Math.*, 9 (1967), 386–393.
- [49] J. H. Wilkinson, *Numer. Math.*, 4 (1962), 368–376.
- [50] J. H. Wilkinson, in: *The Algebraic Eigenvalue Problem*, Clarendon University, Oxford, 1965, pp. 345.
- [51] S. D. Conte and C. deBoor, *Elementary Numerical Analysis*, McGraw-Hill, New York, 1972.
- [52] M. Protopapas, C. H. Keitel and P. L. Knight, *Rep. Prog. Phys.*, 60 (1997), 389–486.
- [53] J. T. Zhang and Takashi Nakajima, *Phys. Rev. A*, 75 (2007), 043403.
- [54] S. V. Khristenko and S. I. Vetchinkin, *Opt. Spektrosk.*, 40 (1976), 417–432.
- [55] S. I. Chu and J. Cooper, *Phys. Rev. A*, 32 (1985), 2769–2775.
- [56] L. V. Keldysh, *ZhEksp. Teor. Fiz.*, 47 (1964), 1945–1957 [*Sov. Phys. JETP*, 20 (1965), 1307–1314].
- [57] P. H. Bucksbaum et al., *Phys. Rev. Lett.*, 56 (1986), 2590–2593.
- [58] Y. Gontier and M. Trahin, *J. Phys. B*, 13 (1980), 4383.
- [59] F. Yergeau, G. Petite and P. Agostini, *J. Phys. B*, 19 (1986), L663.